

A&A manuscript no.

(will be inserted by hand later)

Your thesaurus codes are:

06 (08.09.2 NX Pup; 08.16.5; 09.01.1; 03.20.3)

ASTRONOMY
AND
ASTROPHYSICS
15.9.2018

Simultaneous optical speckle masking and NIR adaptive optics imaging of the 126 mas Herbig Ae/Be binary star NX Puppis^{*}

Markus Schöller¹, Wolfgang Brandner², Thomas Lehmann³, Gerd Weigelt¹, and Hans Zinnecker⁴

¹ Max-Planck-Institut für Radioastronomie, Auf dem Hügel 69, D-53121 Bonn, Germany
ms@speklec.mpifr-bonn.mpg.de, weigelt@mpifr-bonn.mpg.de

² Astronomisches Institut der Universität Würzburg, Am Hubland, D-97074 Würzburg, Germany
brandner@astro.uni-wuerzburg.de

³ Astrophysikalisches Institut und Universitäts-Sternwarte Jena, Schillergäßchen 2, D-07740 Jena, Germany
lehmi@sol.astro.uni-jena.de

⁴ Astrophysikalisches Institut Potsdam, An der Sternwarte 16, D-14882 Potsdam, Germany
hzinnecker@aip.de

Received date; accepted date

Abstract. We present simultaneous optical and near-infrared high angular resolution observations of the close Herbig Ae/Be binary star NX Pup which is associated with cometary globule 1. The reconstructed images have a diffraction-limited resolution of 62 mas in V, 75 mas in R (speckle masking reconstruction), and 115 mas in H, 156 mas in K (adaptive optics + post-processing). Compared to previous results we were able to derive better estimates on spectral type and luminosity and hence put better constraints on the evolutionary status (mass & age) of NX Pup A and B: with NX Pup A of spectral type F0-F2 we estimate the spectral type of NX Pup B in the range F7-G4, masses of $2 M_{\odot}$ and $1.6-1.9 M_{\odot}$, respectively, and an age of 3–5 Myr for both stars.

We discuss the implication of the new age determination on the physical relation between NX Pup and the cometary globule. The dynamical lifetime of $\approx 10^6$ yr for cometary globule 1 suggests that cometary globule 1 and the nearby cometary globule 2 represent transient phenomena and are left overs of a larger molecular cloud which in turn was the parental cloud of NX Pup A and B and finally got dispersed by photoevaporation.

The IR excess of NX Pup A can be modeled by a viscous accretion disk, which is cut off at ≈ 20 AU from the star. NX Pup B has a smaller IR excess which indicates that there is less circumstellar material present than around the primary.

Key words: image processing – interferometry – observational methods: speckle imaging, adaptive optics – Herbig Ae/Be stars: individual: NX Pup

1. Introduction

NX Puppis is a Herbig Ae/Be star (Irvine 1975) associated with cometary globule 1 (CG1, e.g. Harju et al. 1990) which itself is located in the Gum nebula at a distance of ≈ 450 pc (Smith 1968, Brandt et al. 1971, Herbst 1977). NX Pup shows a strong UV excess (de Boer 1977) and IR excess (e.g. Brand et al. 1983). Hoffmeister (1949) was the first to notice it as a highly variable star. The photometric variability has been studied extensively by Bibo & Thé (1991). They found NX Pup to be unique in the sense that the dependence of colour index on magnitude could neither be described as monotonic nor non-monotonic. In Fig. 1 we have plotted the y (in the Strömrgren photometric system) light curve of NX Pup from 1983 till 1995 and the corresponding colour-magnitude diagram, compiled from LTPV data (Long-Term Photometry of Variables Project, Manfroid et al. 1991 & 1995; Sterken et al. 1993 & 1995) and our own data.

The binary nature of NX Pup was first revealed by observations with the Fine Guidance Sensors (FGS) aboard the Hubble Space Telescope (HST) (Bernacca et al. 1993). Follow-up observations of this close Herbig Ae/Be binary (126mas, ≈ 60 AU) were carried out by Brandner et al. (1995) using adaptive optics in the near-infrared. They found that the two components NX Pup A & B are very likely pre-main sequence stars both exhibiting an IR excess. Furthermore, they assigned for component A a spectral type A7–F2, an age of 5×10^6 yr, and a mass of $\approx 2 M_{\odot}$, whereas the physical parameters for component B were more uncertain because of the lack of high angular resolution data in the optical. The spectral type of NX Pup B lies in the range of F5 to G8, the age is between 0.3 and 5×10^6 yr, and the mass is between $\approx 1.5 M_{\odot}$ and $2.5 M_{\odot}$.

Send offprint requests to: M. Schöller

^{*} Based on observations obtained at the European Southern Observatory, La Silla

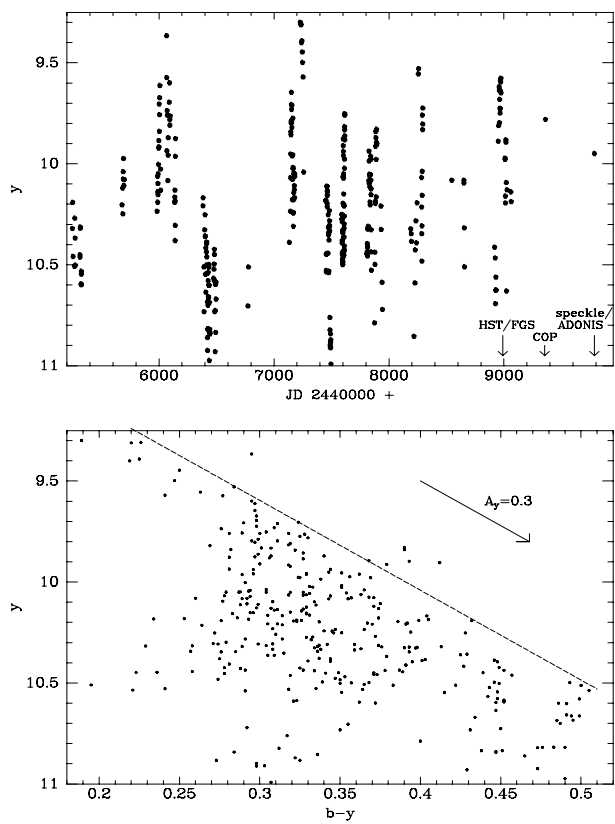


Fig. 1. y (in the Strömgren photometric system) light curve (top) and corresponding y vs. $b-y$ CMD (bottom) of NX Pup from 1983 to 1995 (compiled from LTPV data). Note the rapid variations with an amplitude of $\approx 1^m.7$. Marked by an arrow are the dates of the HST/FGS observations, the first NIR adaptive optics observations (COP), and the current simultaneous data sets presented in this paper. At the time of all three high angular resolution observations NX Pup was relatively bright. The CMD shows no clear colour–magnitude relation. However, the envelope (dashed line) is parallel to the reddening arrow (assuming a standard interstellar extinction law), which indicates that variable extinction is an important constituent of the overall brightness variations.

The age and mass determinations for both components were also uncertain because of the variability of NX Pup and the time gap between the different sets of observations: the adaptive optics JHK observations were carried out exactly one year after the 550 nm (“V”) HST/FGS observations (cf. Fig. 1). Furthermore, the HST observation provided only the brightness difference between the two components but no absolute calibration. The brightness of NX Pup at the time of the HST observation could only be estimated by interpolation of photometric measurements before and after the HST observation.

To remedy this situation, we initiated simultaneous optical and NIR high spatial resolution observations of NX Pup with the aim of obtaining estimates for the binary components in order to put better constraints on their evolutionary status and to probe the circumstellar matter. Furthermore we intended to find clues about the relation of NX Pup to CG1.

All optical and infrared data were obtained within 3 hr between 00:15 and 03:15 UT on Mar 11 1995 (cf. Table 1) which ensures that the variability of NX Pup should affect our conclusions to only a small extent.

2. Observations and data reduction

2.1. Speckle masking results

The NX Pup speckle data were obtained with the ESO/MPG 2.2m telescope at La Silla on March 10/11, 1995. Table 1 gives an overview of the four speckle data sets which were recorded. The FWHM diameter of the motion-compensated long-exposure image was about $0.5''$.

The speckle raw data were recorded with the speckle camera described by Baier & Weigelt (1983). The detector used for the observations was an image intensifier (gain 500 000, quantum efficiency about 10 % at 545 nm and about 8 % at 656 nm) coupled optically to a fast CCD camera (512^2 pixels/frame, frame rate 4 frames/sec, digital correlated double sampling). A system of Digital Signal Processors was used for real-time speckle interferometry and real-time speckle masking, and for fast simultaneous data storage on four Exabyte streamers.

Fig. 2. Diffraction-limited V, R, and H_α speckle masking reconstructions and H-band adaptive optics image of NX Pup. The faint pattern north of NX Pup in the H_α - and H-band image very likely is an artefact.

Fig. 3. Surface plot of the R (FWHM 30 nm, top) and H_α (FWHM 4 nm, bottom) speckle masking reconstruction of NX Pup. The intensity ratio is ≈ 0.620 in the R image and ≈ 0.375 in the H_α image. The images show that even in the 4 nm H_α reconstruction the height of the strongest noise peaks is much smaller than the difference of the R and H_α intensity ratio.

A diffraction-limited image (cf. Fig. 2) of NX Pup was reconstructed from the speckle interferograms by the speckle masking method (Weigelt 1977; Lohmann et al. 1983; Hofmann & Weigelt 1988). The following processing steps were applied to each of the four speckle data sets:

1. Subtraction of the average CCD noise bias and division by the flatfield for each speckle interferogram
2. Calculation of the average power spectrum of all speckle data
3. Subtraction of detector noise bias terms from the average power spectrum
4. Compensation of the photon bias terms in the average power spectrum
5. Calculation of the average bispectrum of all speckle interferograms

Table 1. Journal of observations

telescope/instrument	date (UT)	filter (λ_c , FWHM)	exposure time
D1.54/CCD-camera	11 March 1995 (01:30)	B,V,R	5s, 2s, 1.5s
ESO/MPG 2.2m/speckle camera	11 March 1995 (01:15)	“V” (545nm, 30nm)	629× 50ms
ESO/MPG 2.2m/speckle camera	11 March 1995 (00:15, 03:00)	“R” (656nm, 60nm)	1927× 70ms
ESO/MPG 2.2m/speckle camera	11 March 1995 (01:00, 02:45)	“R” (656nm, 30nm)	2285× 70ms
ESO/MPG 2.2m/speckle camera	11 March 1995 (03:15)	H α (656.3nm, 4nm)	1903× 70ms
ESO3.6m/ADONIS+SHARP	11 March 1995 (02:30)	H, K	400× 0.5s (each)

6. Subtraction of detector noise bias terms from the average bispectrum
7. Compensation of the photon bias terms in the average bispectrum
8. Compensation of the speckle interferometry transfer function in the bias-compensated average power spectrum to obtain the Fourier modulus (Labeyrie 1970)
9. Retrieval of Fourier phase from the bias-compensated average bispectrum
10. Reconstruction of the diffraction-limited image from the object modulus and phase

The photon bias terms in the average power spectrum and bispectrum (due to the spatially extended photoevents of our image intensifier) were compensated by the method described by Pehlemann et al. (1992). The object Fourier phase was reconstructed from the bias-compensated average bispectrum using the conventional phase recursion method (Lohmann et al. 1983).

The bispectrum of each frame consisted of ≈ 35 Million elements (maximum length of bispectrum vectors: maximum u-vector 50 pixels, maximum v-vector 98 pixels, diffraction cut-off frequency at pixel 98) for the R and H α filter data sets. For the V filter data set the bispectrum consisted of ≈ 59 Million elements (maximum length of bispectrum vectors: maximum u-vector 55 pixels, maximum v-vector 113 pixels, diffraction cut-off frequency at pixel 113). Each bispectrum element was weighted with its signal-to-noise ratio (SNR) for correct weighting in the phase recursion algorithm.

Figures 2 and 3 show the results of our speckle observations of NX Pup. No postprocessing by an image restoration method was applied to the speckle masking reconstructions. The reconstructed images have diffraction-limited resolution of 62 mas in V and 75 mas in R.

Table 2. NX Pup parameters derived from the speckle masking observations at epoch 1995.19

filter (λ_c /FWHM)	Separation	PA	Intensity ratio
narrow V (545/30)	128 ± 3 mas	62° 1 ± 1.7	0.537 ± 0.030
broad R (656/60)	124 ± 3 mas	63° 8 ± 1.7	0.620 ± 0.025
narrow R (656/30)	125 ± 3 mas	62° 6 ± 1.7	0.625 ± 0.020
H α (656/4)	122 ± 3 mas	61° 1 ± 1.7	0.375 ± 0.040

A surface plot of the R and H α image is shown in Fig. 3. NX Pup A is significantly brighter than NX Pup B in H α . The intensity ratio, separation, and position angle (PA) of the two components of NX Pup were determined using the IRAF package APPHOT (cf. Table 2).

2.2. Photometric calibration

CCD photometry of the unresolved pair NX Pup A/B was carried out at the Danish 1.5m telescope at La Silla. Observations of standard stars taken from the list by Landolt (1992) allowed for the absolute photometric calibration.

Table 3. Optical and NIR photometry (11 March 1995) and IRAS measurements for component A and B. If only one value is given, it corresponds to the combined (unresolved) brightness/flux of both components.

filter	NX Pup A	NX Pup B
B	10 ^m 35±0 ^m 02	
V	10 ^m 43±0 ^m 05	11 ^m 11±0 ^m 05
R	10 ^m 13±0 ^m 05	10 ^m 64±0 ^m 05
H α ^a	8 ^m 98±0 ^m 10	10 ^m 04±0 ^m 10
J ^b	8 ^m 58±0 ^m 05	9 ^m 56±0 ^m 05
H	7 ^m 47±0 ^m 05	8 ^m 26±0 ^m 05
K	6 ^m 34±0 ^m 05	7 ^m 66±0 ^m 05
12 μ m	7±0.5 Jy	
25 μ m	10±1 Jy	
60 μ m	24±2 Jy	
100 μ m	70±5 Jy	

^a See discussion of the problem concerning the uncertainties in calibrating the H α filter in the text.

^b 1.1.1994 (Brandner et al. 1995)

The 545 nm and 656 nm continuum filters used for the speckle observations are somewhat distinct from the Bessell V and Cousin R filters used in our CCD observations. The speckle “V” filter has the same central wavelength but is about 4 times narrower than the standard filter. For the speckle “R” filter the central wavelength is off by about 10 nm. Hence, we expect systematic errors due to this mismatch of passbands in V smaller than 0.01 mag and in R up to 0.05 mag (depending on the spectral type of the observed object). This effect, however,

will be neglected in the following. For the H_α speckle images no direct photometric calibration was available. However, the ratio of the passbands of the narrowband H_α filter 656/4 and the broadband R filter 656/60 is 1:13.5. While for the H_α observations the stop number of the coupling optics behind the image intensifier was set to 2.0, it was set to 2.8 for the R observations. Hence we get an efficiency ratio of 1:7 between the H_α and the broadband R observations, which is also confirmed by analysing flatfield data. The H_α brightness can be defined by postulating that stars without H_α emission or absorption should have $R-H_\alpha=0$. NX Pup appears to be about 0.4 mag brighter in H_α compared to the H_α brightness observed by Brandner et al. (1995). This can be explained by a brightening of the H_α emission from NX Pup. However, it is still possible that our indirect calibration of the H_α brightness is not perfect. So far we can only say that both stars show H_α in emission, that the majority of the H_α excess originates in NX Pup A, and that this excess is possibly related to the circumstellar matter present around NX Pup A.

All photometric reductions were done using IRAF. The results are summarized in Table 3.

2.3. Adaptive optics imaging

The adaptive optics data were obtained at the ESO 3.6 m using ADONIS (ADaptive Optics Near Infrared System, e.g., Beuzit et al. 1994) in combination with the SHARP (System for High Angular Resolution Pictures, e.g., Hofmann et al. 1995) camera, operated by the Max Planck Institute for Extraterrestrial Physics. NX Pup was observed in the H and K band with a total integration time of 200 s each. Immediately after NX Pup a nearby single star with similar brightness and spectral characteristics was observed as a point source reference.

The data were sky subtracted and flat fielded (using dome flats) following the standard reduction procedure. Stars out of the ISO list of photometric standards (Bouchet, private comm.) were observed several times throughout the night for extinction determinations and absolute photometric calibrations.

The close binary (sep. = $0''.126$) is already clearly resolved on the best single exposures. In order to improve the spatial resolution we selected those 10% of the exposures with the highest Strehl ratio (see also the discussion in Brandner et al. 1995) and coadded them.

As adaptive optics systems only partially compensate the wavefront distortions, the uncompensated power forms a halo around each object. However, at the time of the observations ADONIS did not allow for a direct (simultaneous to the scientific observations) determination of the (instrumental) point spread function (PSF). Therefore a single star had to be observed before and after the scientific observations in order to obtain a PSF calibration. In order to remove the uncompensated halo, the same selection criteria that we used for NX Pup were also applied to the PSF star. The instrumental signature was then (partially) removed by applying two iterations of a “simple deconvolution” (Blecha & Richard 1989). The achieved resolution is 115 mas in H and 154 mas in K. Figure 2 (bottom,

right) shows the H image of NX Pup. The great drawback of this method is that – as observing conditions are changing – the PSF itself is varying and hence no perfect compensation and removal of the instrumental signatures is possible (cf. Fig. 2). The resulting H and K magnitudes can be found in Table 3.

3. Separation, PA, and photometric variability

By averaging the results of the three V and R filter speckle observations we obtain a separation of $126 \text{ mas} \pm 3 \text{ mas}$ and a PA of $62^\circ.8 \pm 1^\circ.7$. These values are in good agreement with previous results obtained by Bernacca et al. (1993, epoch 1993.0: sep. = $126 \pm 7 \text{ mas}$, PA = $63^\circ.4 \pm 1^\circ.0$) and Brandner et al. (1995, epoch 1994.0: sep. = $128 \pm 8 \text{ mas}$, PA = $62^\circ.4 \pm 5^\circ.7$).

Due to the relatively large uncertainty in the determinations of the PA, we still see no evidence for orbital motion. Assuming a system mass of $4 M_\odot$, a semimajor axis of 60 AU (126 mas at 450 pc), and a circular orbit perpendicular to the line of sight we would expect a shift in PA by $\approx 1.5^\circ/\text{yr}$. The lack of such a shift would either mean that our assumptions with respect to the orbital parameters are wrong (i.e. inclination $\neq 0^\circ$ or $e > 0$) or that the distance to NX Pup is considerably larger than 450 pc. Here HIPPARCOS observations – once they are made available – should help to clarify the situation.

Before trying to decompose the spectral energy distribution of NX Pup we have to evaluate what might be the reason for its variability. Different scenarios have been proposed to explain brightness variations in Herbig Ae/Be stars and T Tauri stars: (i) star spots, detected first by Bouvier & Bertout (1989), which can explain quasi-periodic variations observed in weak-line T Tauri stars (ii) solar-type (albeit on a much larger scale) flare events, which can explain the sudden rise in brightness, observed for weak-line T Tauri stars in the optical and in X-rays (e.g. Gahm et al. 1995, Guenther 1995, Preibisch et al. 1995), (iii) variations in the veiling continuum/accretion luminosity, which cause irregular brightness variations in classical T Tauri stars and outburst phenomena like those observed in FUORs and EXORs (e.g. Lehmann et al. 1995), and (iv) variable obscuration by circumstellar material (Grinin 1992) or protoplanets forming in the plane of a circumstellar disk (Thé & Molster 1994).

Recently, Eaton & Herbst (1995) studied UV spectra of 5 UXOR type Herbig Ae/Be stars and gathered evidence that the dominant source of variability is variable extinction. They argue that protoplanets are unlikely responsible for the observed obscuration, because this would require nearly edge-on viewing of the orbits for *all* systems which exhibit this kind of variability.

The general change in colour with brightness is intriguing: the envelope of the CMD in Fig.1 is parallel to the reddening vector, and hence brightness-colour variations along this line can be explained by variable circumstellar extinction. However, near minimum light NX Pup can be as blue as in maximum light. We interpret this as clear evidence for a colour reversal (“blueing effect”, see Wenzel 1969) in some observing periods, especially when NX Pup is faint. The large range of colours of

Table 4. Amplitude of variability of NX Pup

filter	range	ΔM	ref.
u	10 ^m 74–13 ^m 09	2 ^m 3	LTPV
v	9 ^m 79–11 ^m 97	2 ^m 2	LTPV
b	9 ^m 49–11 ^m 46	2 ^m 0	LTPV
y	9 ^m 30–10 ^m 99	1 ^m 7	LTPV
R	9 ^m 46–10 ^m 73	1 ^m 3	BHLWC, R
I	9 ^m 01–10 ^m 28	1 ^m 2	BHLWC, R
J	8 ^m 01–8 ^m 49	0 ^m 5	BHLWC, R
H	6 ^m 94–7 ^m 24	0 ^m 3	BHLWC, R
K	5 ^m 85–6 ^m 06	0 ^m 2	BHLWC, R
L	4 ^m 40–4 ^m 50	0 ^m 1	BHLWC, R

References: BHLWC - Brand et al. 1983, R - Reipurth 1983, LTPV - Sterken et al. 1995

NX Pup at low light level may indicate different strengths of the blueing effect in different observing periods.

By analyzing the lightcurve of NX Pup in short time intervals of good coverage we find the following distinct behaviours: (i) changes in magnitude and colour parallel to the reddening vector when the star is bright, (ii) fast quasiperiodic oscillations (with an amplitude of about 0.6 mag, typical period 14 d) without correlated colour variation, observed when the star exhibits mean or low brightness, (iii) periods of small light variation with little colour change, and (iv) sudden decreases in brightness without any colour change between two periods of small variability.

In general, the timescale of colour variations is much longer than the timescale of intensity variations. Many of the features visible in the brightness and colour of NX Pup have been recorded for other Herbig Ae/Be stars (e.g. HR 5999, Thé 1994) or T Tauri stars (e.g. RY Lup, Gahm et al. 1989, 1993). However, NX Pup is a binary star as well. If we assume that component NX Pup B would not be variable at all, the amplitude of brightness variations for NX Pup A would become considerably larger than the amplitude measured for the unresolved binary system (see Table 4). At low luminosity, also the spread in colours for NX Pup A would increase even more.

The fact that no veiling of photospheric lines has been reported in recent high resolution spectroscopy (Böhm & Catala 1995) supports the variable obscuration scenario rather than models of variable accretion. As, in general, circumstellar extinction dims and reddens the light of a star, we argue – following the reasoning of Gahm et al. (1989) – that the spread in colours at any brightness level (and especially the blueing of NX Pup when it becomes faint) requires an additional source of variability not affected by the obscuration and hence being of circumstellar nature. We propose that the light seen from NX Pup near minimum brightness is mainly scattered light from a circumstellar disk or envelope, while the direct light from the star is heavily obscured. The large range of possible colours at low brightness level of NX Pup could be the result of a variable amount and/or distribution of the scattering particles. The photometric data reveal that the timescale of variability due to

scattered light is of the order of years, whereas occultations and associated quasiperiodic variability occur on timescales of days.

4. SED and the evolutionary status of NX Pup A & B and CG1

Superimposed on the variable obscuration effects, varying accretion luminosity may explain some of the scatter in the CMD. Using IUE spectra (120 nm – 330 nm) of NX Pup, Blondel & Tjin A Dje (1994) could show that the UV spectrum can be decomposed into an underlying stellar photosphere plus accretion luminosity and a viscous accretion disk. Their model consists of a star with a spectral type F2 III–V, a boundary layer with a temperature of $\approx 10^4$ K (resembling the spectrum of an A0 supergiant) and a cool disk. The adopted visual extinction was 0^m4 to 0^m8.

Similar to the decomposition of the UV SED we can try to decompose the optical and infrared SED of NX Pup A & B. Figure 4 shows the overall spectral energy distribution of NX Pup from the UV to the mm–range. The UV values are from de Boer (1977, epoch: 1975.83), the U to K from our own measurements (this paper & Brandner et al. 1995), the L and M values from Hillenbrand et al. 1992, the 12 μ m to 100 μ m IRAS fluxes (cf. Table 3) were measured on FRESCO/HIRES images obtained from the Infrared Processing & Analysis Center (IPAC)¹, and the 1.3 mm value, which represents an upper limit, is from Henning et al. (1994).

Most of the light detected in V and R is emitted by the stellar photospheres of NX Pup A and B. Both components also exhibit a NIR excess. While the SED of NX Pup B peaks at H, the SED of NX Pup A is still rising at K. Hence, the majority of the IR excess arises from component A. The lack of strong emission from cold dust at 1.3 mm, which mainly originates from the cooler outer parts of the disk, suggests that the inner disk around NX Pup A is cut off at about 20 AU and that there is no massive circumbinary disk present. Theoretical calculations of disk sizes (both circumstellar and circumbinary) in binary systems by Papaloizou & Pringle (1977) and Artymowicz & Lubow (1994) indicate that the circumprimary disk may extend out to 0.4 times the semimajor axis of the binary orbit, which for NX Pup is about 20 AU, whereas the circumsecondary disk should be considerably smaller (about 10 AU in our case). The predictions, however, are sensitive to parameters like mass ratio, eccentricity of binary orbit, or viscosity parameter α .

Based on low to intermediate resolution spectroscopy, Brand et al. (1983) and Reipurth (1983) classified NX Pup as F0–F2. Using the spectral type – effective temperature calibration from de Jager & Nieuwenhuijzen (1987) and the colours and bolometric corrections as tabulated by Hartigan et al. (1994) we are able to place NX Pup A in an H-R diagram. If we adopt a MK type of F1 IV–V for NX Pup A, the observed

¹ IPAC data can be retrieved on the WWW via <http://www.ipac.caltech.edu/>

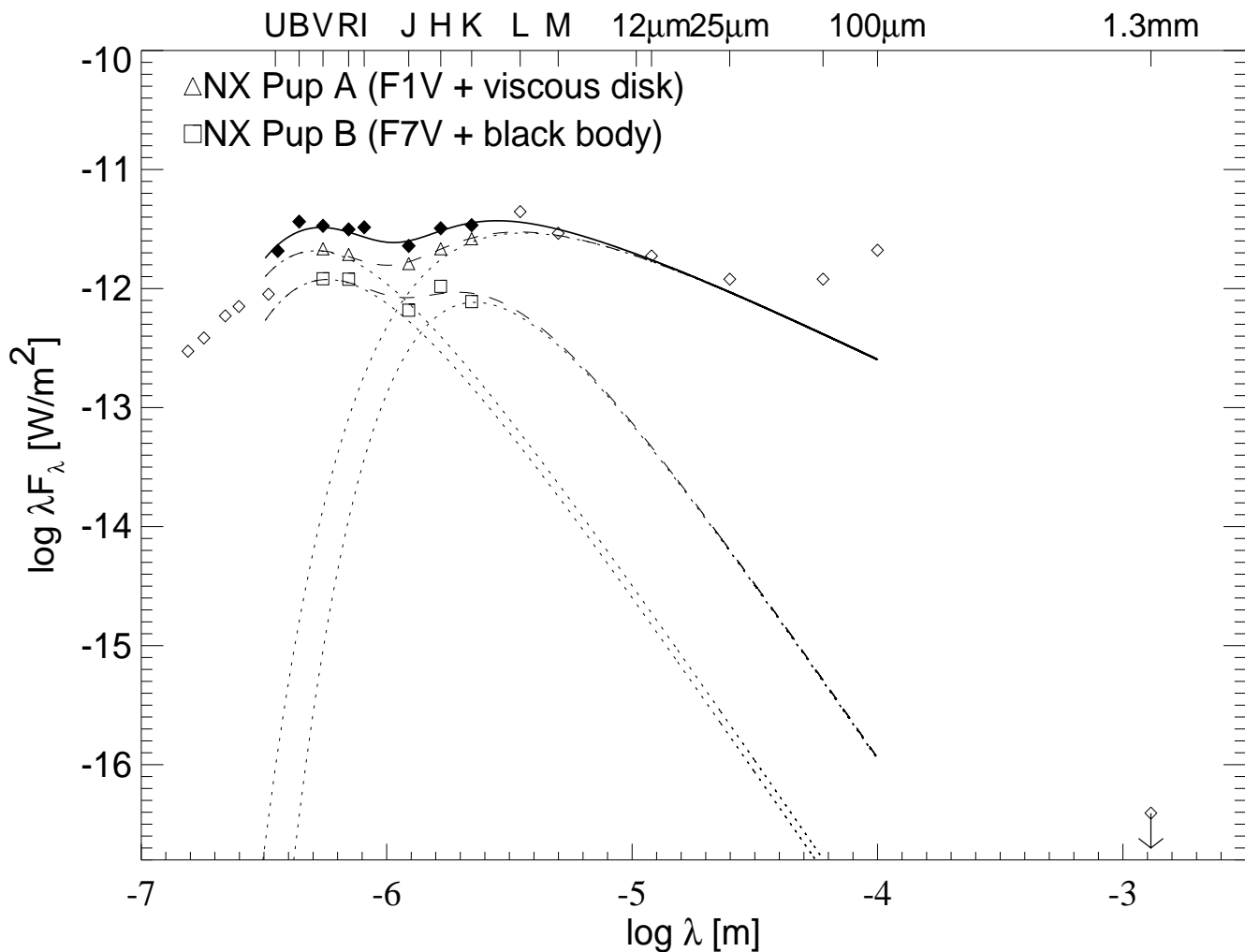


Fig. 4. Dereddened (assuming $A_v = 0^m.48$) spectral energy distribution λF_λ of NX Pup A and B from the UV to the mm-range. The filled diamonds and open triangles indicate our own measurements. The lack of strong 1.3 mm emission suggests that the circumstellar disk around NX Pup A is cut off at about 20 AU and that there is no circumbinary disk present around NX Pup A/B. The total spectral energy distribution can be decomposed into four parts (dotted lines): the photospheric emission from NX Pup A (F1V) and NX Pup B (F7V), a viscous accretion disk around NX Pup A, and circumstellar matter around NX Pup B which is approximated by a blackbody. The dashed lines mark both the SEDs of the individual stellar photospheres plus the IR excess due to circumstellar matter for NX Pup A and B. The overall SED is indicated by a solid line and gives a reasonable fit to the observed flux distribution (diamonds). The errors in flux are 5% or less (see text for more details).

V–R colour ($0^m.30$) yields a visual extinction $A_V \approx 0^m.48$. This value is in good agreement with the value derived by Blondel & Tjin A Djie (1994) from best fits of IUE spectra of NX Pup ($A_v \approx 0^m.43$) and allows us to determine L_{bol} .

By assuming the same extinction for NX Pup B, its V–R colour yields a spectral type F7V. However, the fact that NX Pup B’s IR excess is significantly smaller than that of NX Pup A might indicate that while it suffers the same foreground extinction as NX Pup A, its circumstellar extinction might be considerably less. Studies by Krautter (1980) and Brandt et al. (1971) indicate that the amount of foreground extinction in the direction of the Gum nebula might be as small as $A_v \approx 0^m.15$

out till 500 pc from the Sun. If NX Pup B suffered no additional extinction, its V–R colour would yield a spectral type of G4V. Accordingly, we compute $L_{bol} \approx 7.3 - 9.4 L_\odot$.

Mass and age determinations based on different sets of PMS evolutionary tracks yield similar results. We used theoretical tracks computed by D’Antona & Mazzitelli (1994) and Palla & Stahler (1993), based on different input physics (i.e., opacities and convection models), which are in good agreement for intermediate mass stars older than 10^6 yr (cf. Fig. 5). The results are summarized in Table 5.

What is the relation of NX Pup A & B to CG1? Based on molecular line observations with the SEST Harju et al. (1990)

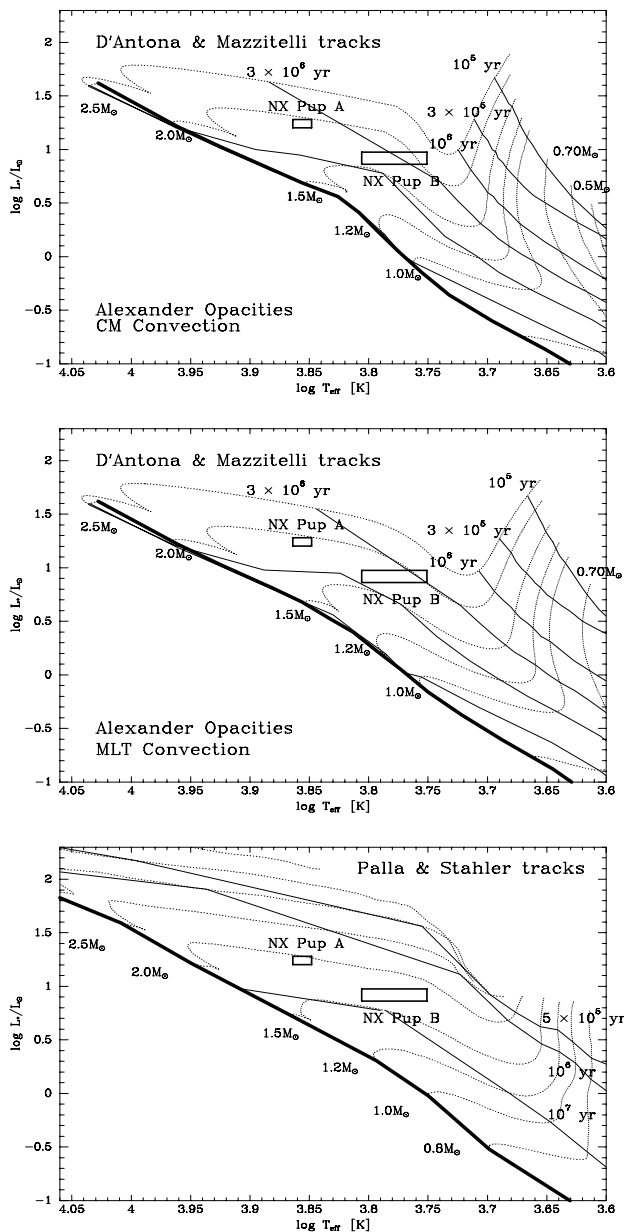


Fig. 5. NX Pup A & B placed on theoretical PMS evolutionary tracks (dotted lines) based on different input physics. The solid lines indicate isochrones and the Zero Age Main Sequence (ZAMS) is marked by a bold solid line. The various tracks are in good agreement for intermediate mass stars (i.e. $1.5 M_{\odot}$ to $2.5 M_{\odot}$) older than 10^6 yr.

show that the kinetic energy within CG1 is too large for the globule to be gravitationally bound. They estimate a dynamical age of the order of 10^6 yr for CG1. Furthermore, they argue that the enhanced $[\text{HCN}]/[\text{HNC}]$ ratio in the head of the globule indicates that a shock front reached CG1 and changed the chemistry within the head. In total 75 % of all cometary globules in the Gum nebula show indications of a shock induced change in their chemistry (presence of ammonia, cf. Bourke et al. 1995) compared to only 40 % of all Bok globules surveyed

Table 5. Evolutionary status of NX Pup A & B

NX Pup	A	B
separation	$0''.126 \pm 0''.003^a$	
PA	$62^\circ.8 \pm 1^\circ.7^a$	
SpT	F0–F2 ^b	F7–G4
L/L_{\odot}	16–19	7–9
mass	$\approx 2 M_{\odot}$	$1.6\text{--}1.9 M_{\odot}$
age	$3\text{--}5 \times 10^6$ yr	$2\text{--}6 \times 10^6$ yr

^a 11.3.1995

^b Brand et al. 1983, Reipurth 1983, Blondel & Tjin A Djie 1994

outside the Gum nebula. Bourke et al. further suggest that the large percentage of ammonia detections and the fact that 50 % of the CGs have an associated IRAS source is a strong indication that star formation is enhanced in CGs compared to Bok globules.

Harju et al. (1990) propose that CG1 and the nearby CG2 might just represent sparse left overs of a single more massive molecular cloud which got slowly dispersed due to photoevaporation. The evaporation was very likely triggered by UV radiation from hot massive stars located near the centre of the Gum nebula. NX Pup A & B may have formed some $3\text{--}5$ Myr ago within this larger single molecular cloud, and hence considerably before CG1 reached its current morphology.

The IR excess of NX Pup A can be approximated by the viscous accretion disk spectrum, first modeled by Lynden–Bell & Pringle (1974), in which F_{λ} falls off $\propto \lambda^{-4/3}$ towards longer wavelength. This rather simple model consists of a thin viscous accretion disk made up of concentric isothermal rings radiating like a black body. We note that an accurate modeling of a physical accretion disk, especially one that is also reprocessing stellar radiation, however, is much more complex and therefore it is not possible to derive parameters of a disk from the spectrum alone (see e.g. Sonnhalter et al. 1995). The non-detection of 1.3 mm dust continuum emission (Henning et al. 1994) suggests that the disk around NX Pup A is cut off at about 20 AU possibly due to the presence of component B (cf. Jensen et al. 1996 for a submm study of PMS binaries and Artymowicz & Lubow 1994 for model calculations). For component B a single black body with a temperature of ≈ 1600 K gives only a crude fit to the observed SED in the NIR. This could mean that there is much less circumstellar matter left around NX Pup B compared to NX Pup A, and that the distribution of matter around NX Pup B is rather inhomogeneous because of the tidal torque of NX Pup A.

Clearly, for both NX Pup A and B more detailed model calculations and spatially resolved imaging towards longer wavelengths are necessary to put better constraints on the structure and geometry of the circumstellar material around each star. Furthermore, high spatial resolution observations of NX Pup near its minimum brightness would be interesting. One would expect that NX Pup A then is completely obscured and would

only be visible in the optical through light scattered by circumstellar material, similar to the active Herbig Ae/Be star Z CMa, where the IR companion was detected in the visual by Barth et al. (1994) and Thiébaud et al. (1995). Measurements of the polarization of NX Pup A & B near minimum brightness would be a test for the scattered light hypothesis.

5. Summary

We have analysed quasi-simultaneous high angular resolution optical speckle and NIR adaptive optics data of the close Herbig Ae/Be binary star NX Pup. Within the observational errors both components appear to be coeval (3–5 Myr) and have masses around $2 M_{\odot}$ and $1.6\text{--}1.9 M_{\odot}$, respectively. NX Pup appears to be older than the current morphological configuration of CG1, which has a dynamical age of only 1 Myr. The circumstellar matter around NX Pup A can be described by a viscous accretion disk out to a distance of ≈ 20 AU from the star. The outer part of the disk, however, seems to be cut-off by the gravitational influence of the secondary. The secondary itself has only a small amount of circumstellar matter left.

Acknowledgements. We are grateful to J.F. Claeskens for providing part of his telescope time at the D1.54m. We thank the LTPV project for making their data available via CDS. We thank P. Bouchet for communicating the list of photometric ISO standards to us. WB & TL were supported by student fellowships of the European Southern Observatory. WB acknowledges support from the Deutsche Forschungsgemeinschaft (DFG) under grant Yo 5/16-1. HZ acknowledges support from the DARA under grant 05 OR 9103 0. This research has made use of the Simbad database, operated at CDS, Strasbourg, France, NASA's Astrophysics Data System (ADS), and the IRAF PACKAGE C128, developed by E. Tessier at the Observatoire de Grenoble.

References

- Artymowicz P., Lubow S.H. 1994, ApJ 421, 651
 Baier, G., Weigelt, G. 1983, A&A 121, 137
 Barth W., Weigelt G., Zinnecker H. 1994, A&A 291, 500
 Bernacca P.L., Lattanzi M.G., Bucciarelli B. et al. 1993, A&A 278, L47
 Beuzit J.-L., Hubin N., Gendron E., et al. 1994, Proc. SPIE 2201, pp. 955-961, M.A. Ealey & F. Merkle (Eds.)
 Bibo E.A., Thé P.S. 1991, A&AS 89, 319
 Blecha, A., Richard, L. 1989, in *1st ESO/ST-ECF Data Analysis Workshop*, p. 209
 Blondel P.F.C., Tjin A Djie H.R.E. 1994, ASP Conf. Ser. 62, P.S. Thé et al. (Eds.), 211
 Böhm T., Catala C. 1995, A&A 301, 155
 de Boer K.S. 1977, A&A 61, 605
 Bourke, T.L., Hyland, A.R., Robinson, G., James, S.D., Wright, C.M. 1995, MNRAS 276, 1067
 Bouvier J., Bertout, C. 1989, A&A 211, 99
 Brand P.W.J.L., Hawarden T.G., Longmore A.J., Williams P.M., Caldwell J.A.R. 1983, MNRAS 203, 215
 Brandner, W., Bouvier J., Grebel E.K. et al. 1995, A&A 298, 818
 Brandt, J.C., Stecher, T.P., Crawford, D.L., Maran, S.P. 1971, ApJ 163, L99
 D'Antona F., Mazzitelli I. 1994, ApJS 90, 467
 Eaton, N.L., Herbst, W. 1995, AJ 110, 2369
 Gahm, G.F., Fischerström, C., Liseau, R., Lindroos, K.P. 1989, A&A 211, 115
 Gahm, G.F., Liseau, R., Gullbring, E., Hartstein D. 1993, A&A 279, 477
 Gahm, G.F., Loden, K., Gullbring, E., Hartstein, D. 1995, A&A 301, 89
 Grinin, V.P. 1992, A&AT 3, 17
 Guenther, E. 1995, AG Abstr. Series 11, 124
 Harju J., Sahu M., Henkel C., et al. 1990, A&A 233, 197
 Hartigan, P., Strom, K.M., Strom, S.E. 1994, ApJ 427, 961
 Henning Th., Launhardt R., Steinacker J., Thamm E. 1994, A&A 291, 546
 Herbst, W. 1977, PASP 89, 795
 Hillenbrand, L., Strom, S.E., Vrba, F.J., Keene, J. 1992, ApJ 397, 613
 Hoffmeister C. 1949, Astr. Abh. Erg. A.N. 12, No. 1
 Hofmann, K.-H., Weigelt, G. 1988, A&A 203, L21
 Hofmann, R., Brandl, B., Eckart, A., Eisenhauer, F., Tacconi-Garman, L., *High-Angular Resolution NIR Astronomy with Large Arrays (SHARP I and SHARP II)*, in: *Infrared Detectors and Instrumentation for Astronomy*, Orlando, ed. A.M.Fowler, SPIE Volume 2475, 192–195, 1995
 Irvine N.J. 1975, PASP 87, 87
 de Jager C., Nieuwenhuijzen H. 1987, A&A 177, 217
 Jensen, E.L.N., Mathieu, R.D., Fuller, G.A. 1996, ApJ, *The Connection between Submillimeter Continuum Flux and Binary Separation* (in press)
 Krautter, J. 1980, A&A 89, 74
 Labeyrie, A. 1970, A&A 6, 85
 Landolt A. 1992, AJ 104, 340
 Lehmann, T., Reipurth B., Brandner, W. 1995, A&A 300, L9
 Lohmann, A., Weigelt, G., Wirtitzer, B. 1983, Appl. Opt. 22, 4028
 Lynden-Bell, D., Pringle, J.E. 1974, MNRAS 168, 603
 Manfroid, J., Sterken, C., Bruch, A., et al. 1991 A&AS 87, 481
 Manfroid, J., Sterken, C., Cunow, B., et al. 1995 A&AS 109, 329
 Palla, F., Stahler, S.W. 1993 ApJ 418, 414
 Papaloizou J.C.B., Pringle J.E. 1977, MNRAS 181, 441
 Pehlemann, E., Hofmann, K.-H., Weigelt, G. 1992, A&A 256, 701
 Preibisch, T., Neuhäuser, R., Alcalá J. 1995, A&A 304, L13
 Reipurth, B. 1983, A&A 117, 183
 Smith, L.F. 1968, MNRAS 140, 409
 Sonnhalter, C., Preibisch, T., Yorke, H.W. 1995, A&A 299, 545
 Sterken, C., Manfroid J., Anton, K., et al. 1993 A&AS 102, 79
 Sterken, C., Manfroid J., Beele, D., et al. 1995 A&AS 113, 31
 Thé P.S. 1994, ASP Conf. Ser. Vol. 62, 23
 Thé P.S., Molster F.J. 1994, Ap&SS 212, 125
 Thiébaud, E., Bouvier, J., Blazit, A., Bonneau, D., Foy, F.-C. 1995, A&A 303, 795
 Weigelt, G. 1977, Optics Commun. 21, 55
 Wenzel W. 1969, in *Non-periodic Phenomena in Variable Stars*, IAU Coll. No. 4, p. 61